[3] K. B. Bhasin *et al.*, "Performance of a YBaCuO superconducting filter/GaAs low noise amplifier hybrid circuit," in *IEEE MTT-S Dig.*, 1992, pp. 481–483.
[4] W. Brockerhoff *et al.*, "RF measurements and characterization of heterostructure field-effect transistors at low temperatures," *IEEE Trans. Microwave Theory Tech.*, vol. 37, pp. 1380–1388, 1989.
[5] V. Iyengar *et al.*, "Low-temperature current drift and its origin in heterostructure and quantum-well MODFET's," in *Proc. 14th Gallium Arsenide Related Compounds*, 1988, pp. 669–672.
[6] J. Kolodzey *et al.*, "Cryogenic temperature performance of modulation-doped field-effect transistors," *Electronic Lett.*, vol. 25, pp. 777–779, 1989.
[7] R. Lai *et al.*, "Characteristics of 0.8- and 0.2-μm gate length $In_xGa_{1-x}As/In_{0.52}Al_{0.48}As/InP$ modulation-doped field-effect transistors at cryogenic temperatures," *IEEE Trans. Electron Devices*, vol. 39, pp. 2206–2213, 1992.
[8] J. W. Smuk, M. G. Stubbs, and J. S Wight, "Vector measurements of microwave devices at cryogenic temperatures," in *IEEE MTT-S Dig.*, 1989, pp. 1195–1198.
[9] Y. Kwark, P. Solomon, and D. La Tulipe, "S-parameter characterization of GaAs gate SISFET's at liquid nitrogen temperatures," in *Proc. IEEE/Cornell Univ. Conf. Advanced Concepts High Speed Dev. Ckts.*, pp. 208–217, 1989.
[10] C. A. Leichti and R. B. Larrick, *IEEE Trans. Microwave Theory Tech.*, vol. MTT-24, pp. 365–370, June 1976.
[11] J. Laskar and J. Kolodzey, "Cryogenic vacuum high frequency probe station," *J. Vac. Sci. Technol.*, vol. B, no. 8, pp. 1161–1165, Sept./Oct. 1990.
[12] J. Laskar and M. Feng, "An on-wafer cryogenic microwave probing system for advanced transistor and superconductor applications," *Microwave J.*, vol. 36, pp. 104–114, Feb. 1993.
[13] H. Meschede *et al.*, "On-wafer microwave measurement setup for investigations on HEMT's and high-T_c superconductors at cryogenic temperatures down to 20 K," *IEEE Trans. Microwave Theory Tech.*, vol. 40, pp. 2325–2331, 1992.
[14] R. B. Marks, "A multiline method of network analyzer calibration," *IEEE Trans. Microwave Theory Tech.*, vol. 39, pp. 1205–1215, 1991.
[15] D. F. Williams and R. B. Marks, "Accurate transmission line characterization," *IEEE Microwave Guided Wave Lett.*, vol. 3, pp. 247–249, 1993.
[16] M. Golio, W. Seely, and D. Halchin, "Spreadsheet program extracts transistor parasitic elements," *Microwaves RF*, pp. 67–73, Oct. 1992.
[17] M. Berroth and R. Bosch, "Broad-band determination of the FET small-signal equivalent circuit," *IEEE Trans. Microwave Theory Tech.*, vol. 38, no. 7, pp. 891–895, 1990.
[18] G. Dambrine *et al.*, "A new method for determining the FET small-signal equivalent circuit," *IEEE Trans. Microwave Theory Tech.*, vol. 36, no. 7, pp. 1151–1159, 1988.
[19] P. White and R. M. Healy, "Improved equivalent circuit for determination of MESFET and HEMT parasitic capacitances from 'Coldfet' measurements," *IEEE Microwave Guided Wave Lett.*, vol. 3, no. 12, pp. 453–454, Dec. 1993.
[20] M. Pospiezalski, "Modeling of noise parameters of MESFET's and MODFET's and their frequency and temperature dependence," *IEEE Trans. Microwave Theory Tech.*, vol. 37, pp. 1340–1350, 1989.
[21] S. Weinreb, R. Harris, and M. Rothman, "Millimeter-wave noise parameters of high-performance HEMT's at 300 K and 17 K," in *IEEE MTT-S Dig.*, 1989, pp. 813–816.
[22] M. W. Pospieszalski, "Cryogenically-cooled, HFET amplifiers and receivers: State-of-the-art and future," in *IEEE MTT-S Dig.*, 1992, pp. 1369–1372.
[23] M. W. Pospieszalski and A. C. Niedzwiecki, "FET noise model and on-wafer measurement of noise parameters," in *IEEE MTT-S Dig.*, 1991, pp. 1117–1122.

Radial Mode Matching Analysis of Ridged Circular Waveguides

Uma Balaji and Ruediger Vahldieck

***Abstract*—In this paper a radial mode matching analysis is presented to calculate rigorously the TE and TM mode propagation in single- double-, triple-, and quadruple-ridged circular waveguide structures. The ridges have been cut radially in all the cases. Results are presented for variations of the ridge depth and ridge thickness and are compared to results from finite element analysis. Furthermore, for the first time, the characteristic impedance of the double and quadruple-ridged circular waveguides have been calculated using the power-voltage definition.**

I. Introduction

Various numerical techniques have been applied in the past to solve the eigenvalue problem of single- [1], double- [2]–[4], triple- [5], [6], and quadruple-ridged [4], [7], [8] circular waveguides with ridges of uniform thickness or ridges that are radially cut. Most of the above work is based on the discretization of the space or space and time to solve the Helmholtz equation. To avoid memory consuming space discretization techniques, a radial mode matching method has been developed [14] for the analysis of single- and double-ridged circular waveguides. The method is extended here to triple- and quadruple-ridged circular waveguides. In order to avoid mixed coordinate systems which occur when rectangular ridges are utilized in a cylindrical waveguide, the ridges are assumed to be conically shaped [10]. Mechanically, they are as simple to fabricate as the more traditional rectangular ridges. The approach developed in the following is rigorous and can be applied to symmetrical as well as asymmetrical structures.

II. Theory

1) Eigenvalue Problem: To start with we first consider the cross section of the single-ridged circular waveguide of Fig. 1(a) and (b). The double- and quadruple-ridged circular waveguide can be easily derived from the following theory by considering electric wall (ew) and magnetic wall (mw) symmetry. The eigenvalues of the orthogonal dominant modes and higher order modes of such a structure can be obtained from the solution of the Helmholtz equation in cylindrical coordinates.

Solving the Helmholtz equation in each homogeneous subregion and considering the boundary condition, the potential function for regions 1 and 2 for TE modes can be written as follows:

$$\psi^{(1)} = \sum_{n=r}^{N1} A_n J_n(k_c\rho) \begin{cases} \sin n\phi & r = 1 \text{ for mw} \\ \cos n\phi & r = 0 \text{ for ew} \end{cases} \tag{1}$$

$$\psi^{(2)} = \sum_{m=r}^{N2} C_m [H_l^{(2)'}(k_c b) H_l^{(1)}(k_c\rho) - H_l^{(1)'}(k_c b) H_l^{(2)}(k_c\rho)] \cdot \begin{cases} \cos l(\phi-\theta) & r = 1, 3 \text{ and } l = \dfrac{m\pi}{2(\pi-\theta)} \text{ for mw} \\ \cos l(\phi-\theta) & r = 0 \text{ and } l = \dfrac{m\pi}{\pi-\theta} \text{ for ew.} \end{cases} \tag{2}$$

Manuscript received October 3, 1995; revised March 20, 1996.

The authors are with the Department of Electrical and Computer Engineering, University of Victoria, Victoria, British Columbia, V8W 3P6 Canada.

Publisher Item Identifier S 0018-9480(96)04729-1.

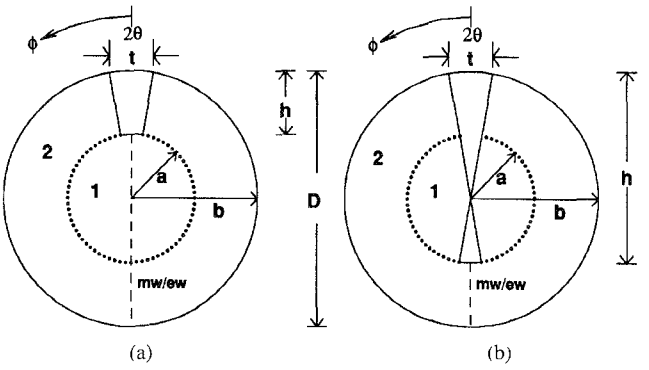

Fig. 1. Geometry of a single-ridged circular waveguide (a) ridge depth < radius and (b) ridge depth > radius.

The functions J_n are the Bessel functions of order n and H_l are the Hankel functions of order l. The unknown coefficients of the eigenfunctions are A_n and C_m and b is the radius of the circular waveguide. The special case of ridge depth equal to the radius has been treated in [13]. For the special case with ridge depth larger than the radius, the potential functions for the TE modes in the region 2 is the same as (2), while for region 1 it is given below

$$\psi^{(1)} = \sum_{n=0}^{N1} A_n J_q(k_c\rho) \cos \frac{n\pi(\phi-\theta)}{\pi-2\theta} \tag{3}$$

where $q = (n\pi)/(\pi-2\theta)$.The potential functions for the TM modes for both symmetries can be written in a similar form.

From the potential functions, the field components in each of the regions can be derived. Equating E_ϕ and H_z for TE modes and E_z and H_ϕ for TM modes at the interface of the two subregions and using the orthogonality property, a system of linear equations of infinite size as a function of k_c is obtained. The size of this system of equations is made finite depending on the truncation index $N1$ and $N2$. The ratio between $N1$ and $N2$ is chosen to be close to the ratio of the angular widths of region 1 and region 2 to avoid relative convergence problems [9]. However, for the case of thin ridges the value of $N1 = N2$. The eigenvalues of the system of equations $[F][x] = 0$ are obtained either by searching for minimum singular value of the characteristic matrix $[F]$ or by searching for the zeros of the determinant (det $[F] = 0$). Since matrix singular value decomposition offers more accurate and pole free solutions [11], this technique has been chosen here for evaluation of the eigenvalues.

For the double- and quadruple-ridged circular waveguide an additional symmetry is considered making it possible to analyze only one quarter of the cross section.

2) Characteristic Impedance: The characteristic impedance of the ridged circular waveguide can be obtained using the power-voltage definition $[Z_o = V^2/2P]$. The slot voltage V for the double-ridged and quadruple-ridged waveguide can be obtained from the electric field along the slot. For the fundamental mode, the slot voltage is obtained by evaluating the integral numerically in the equation below

$$V = -2\int_0^a J_1(k_c\rho)\frac{1}{\rho}\,d\rho \tag{4}$$

The coefficient of the potential function corresponding to the fundamental mode in region 1 is assumed unity. Then the coefficients for the fields in subregion 2 for the fundamental mode are evaluated by solving the homogeneous characteristic equation for a given k_c. The average power transported in the quarter cross-section of the ridged guide is determined from the sum of the average power flowing in the subregions (1) and (2). The total average power P is four times this sum. For example, the power in region 1 for the fundamental mode is given as

$$P^{(1)} = \frac{\beta}{2\omega\mu}\int_0^a\int_0^{\pi/2}\left[\frac{1}{\rho^2}J_1^2(k_c\rho)\cos^2\phi + J_1'^2(k_c\rho)\sin^2\phi\right]\rho\,d\rho\,d\phi. \tag{5}$$

A similar expression is obtained for the power in region 2.

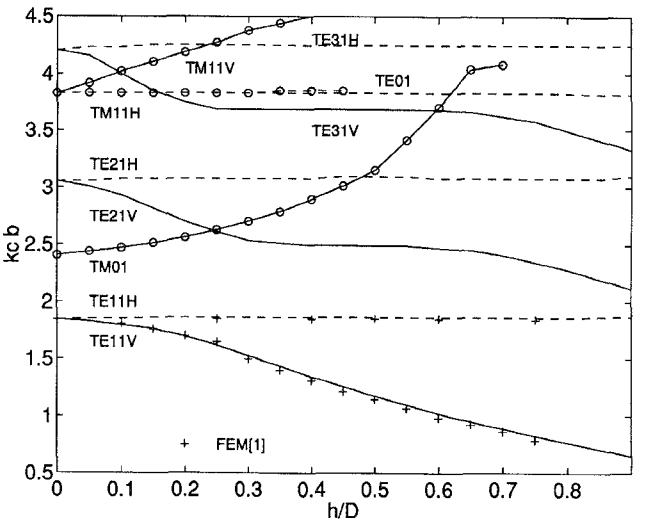

Fig. 2. Cutoff characteristics of single-ridged circular waveguide ($t/D = 0.04$)

III. Results

The nomenclature of $TE_{n,m}$ and $TM_{n,m}$ modes of the empty circular waveguide is maintained even though the presence of metallic ridges distorts the field distribution of these modes. Using the above mode nomenclature means nothing else than that those modes can be traced back to the corresponding ones in the empty (undisturbed) circular waveguide.

Fig. 2 shows the cutoff characteristics of a single-ridged circular waveguide. The results of the fundamental mode have been compared with a finite element solution [1] and good agreement was found. Since, the ridge is positioned to load either inductively or capacitively for the orthogonal polarizations of the TE modes, mode splitting occurs. The mode splitting phenomenon for TE and TM modes is represented as V (Vertical polarization or magnetic wall symmetry) and H (Horizontal polarization or electric wall symmetry) in the figures. In [1] it was reported that the low port isolation of a septum polarizer was due to the onset of the $TM_{0,1}$ mode. However, as Fig. 2 clearly shows, exceeding certain ridge penetration depth the cutoff frequency of the $TE_{2,1}$ V mode is lower than that of the $TM_{0,1}$ and it is rather this mode that is responsible for the limited port isolation reported in [1].

The variation of the cut off frequency of the fundamental and higher order modes with respect to ridge penetration depth in a double-ridged circular waveguide is shown in Fig. 3. Mode splitting of the orthogonally polarized $TE_{1,1}$, $TE_{2,1}$ and $TM_{1,1}$ modes is clearly shown. The splitting of these modes is due to the same reasons as explained for the single-ridged waveguide.

For a quadruple-ridged waveguide with identical ridge depths, the cutoff characteristics for the fundamental and higher order modes is shown in Fig. 4. The modes with magnetic wall along one line of symmetry and electric wall along the other ($TE_{1,1}$, $TE_{3,1}$, $TE_{1,2}$, etc.; $TM_{1,1}$, $TM_{3,1}$, etc. or in general $TE_{2m+1,n}/TM_{2m+1,n}$)

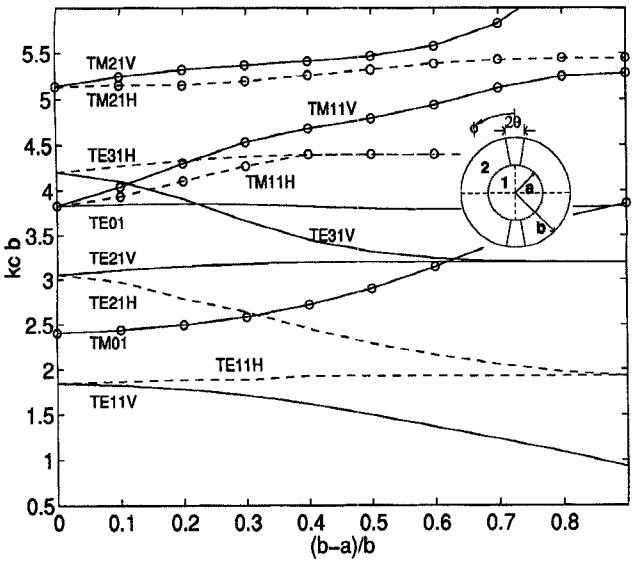

Fig. 3. Cutoff characteristics of double-ridged circular waveguide, ridge thickness $(2\theta) = 10°$.

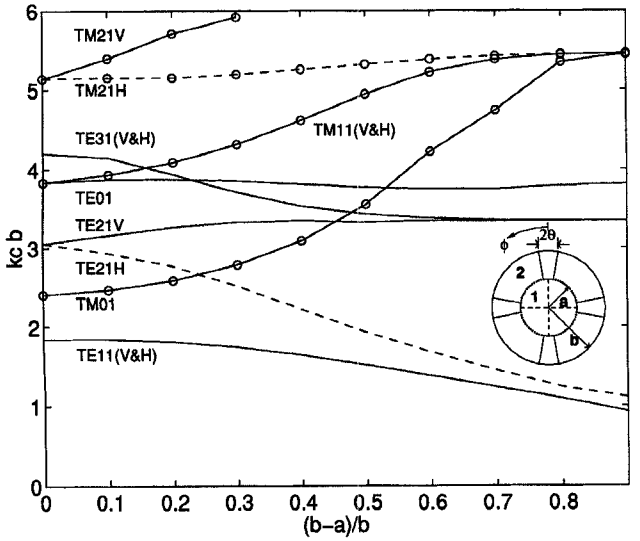

Fig. 4. Cutoff characteristics of quadruple-ridged circular waveguide, ridge thickness $(2\theta) = 10°$.

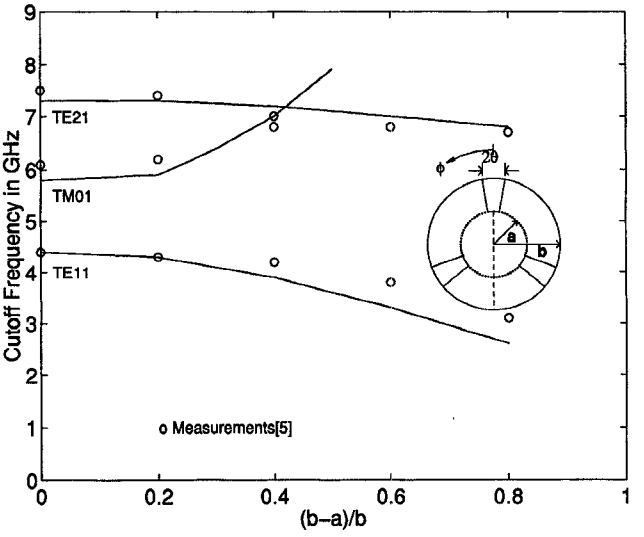

Fig. 5. Cutoff characteristic of triple-ridged circular waveguide, $b = 2$ cm, ridge thickness $(2\theta) = 20°$.

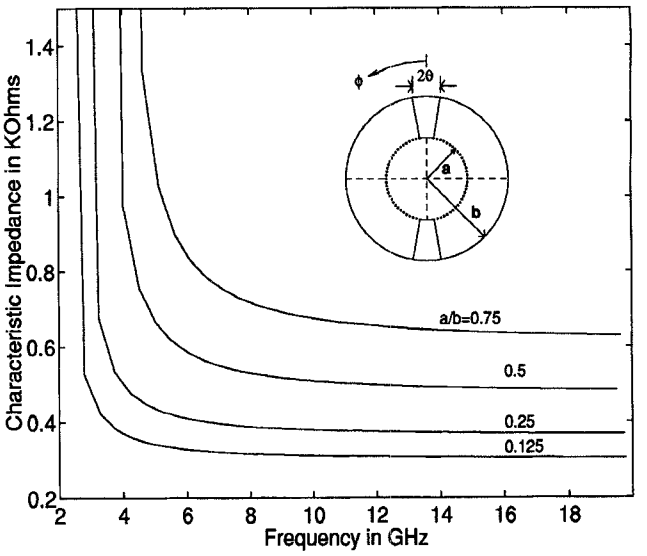

Fig. 6. Characteristic impedance of double-ridged circular waveguide, $b = 2$ cm, ridge thickness $(2\theta) = 10°$.

have the same structure for both polarizations and hence the same eigenvalues. In contrast, the modes such as $TE_{2,1}$, $TE_{4,1}$, and $TE_{2,2}$ (in general, $TE_{2m,n}$) will have either electric or magnetic walls along both lines of symmetry for the orthogonal polarization and therefore the loading by the ridges is either inductive or capacitive and mode splitting occurs. In comparison to the single-ridge and double-ridge case, the loading is higher because of the presence of additional ridges and hence the cutoff frequencies of such modes increase or decrease more rapidly. Similarly, modes like $TM_{2,1}$, $TM_{4,1}$, and $TM_{2,2}$ (modes with electric or magnetic walls along both lines of symmetry) do split up which is a phenomenon that has not been reported in [7], [8]. But unlike for TE modes, the loading by the ridges is always inductive for TM modes and the loading is higher in comparison to the single and double-ridged waveguide due to the presence of the additional ridges.

The cut off frequency variation of a triple-ridged circular waveguide versus ridge penetration depth is shown in Fig. 5. A good agreement with measurements [5] is observed. The bandwidth of the triple-ridged circular waveguide is the largest of all the cases investigated since the orthogonal polarizations are degenerate.

The characteristic impedance of double- and quadruple-ridged circular waveguide has not been investigated in the literature before but is of practical importance in the design of related components [12]. The characteristic impedance of double-ridged circular waveguide for various penetration depth for vertical polarization is shown in Fig. 6. The variation of characteristic impedance of the quadruple-ridged circular waveguide with the ridge penetration depth at three different frequencies is shown in Fig. 7. In comparison to the double-ridged circular waveguide, the characteristic impedance of the quadruple-ridged waveguide with the increased ridge penetration depth is slightly lower because of the presence of the two additional ridges.

IV. Conclusion

The radial mode matching method has been utilized in the analysis of cutoff characteristics for a family of ridged circular waveguides.

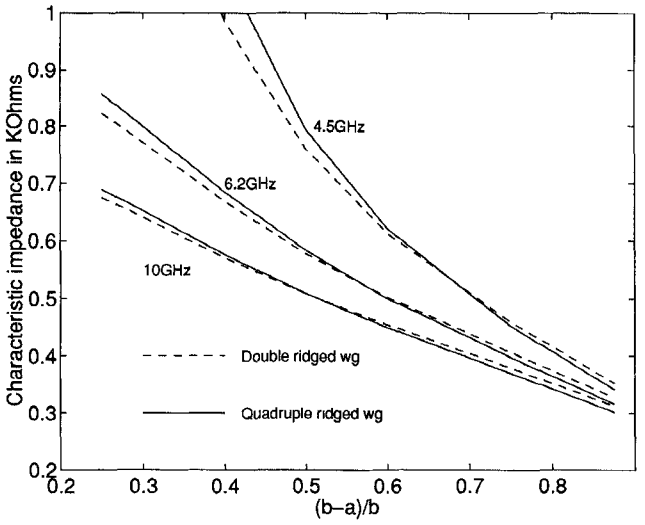

Fig. 7. Characteristics impedance of quadruple and double-ridged circular waveguide versus ridge depth, $b = 2$ cm, ridge thickness $(2\theta) = 10°$.

Mode splitting phenomena are observed for the TE and TM modes in single-, double- and quadruple-ridged circular waveguides but not in triple-ridged circular waveguides. The triple-ridged circular waveguide has the largest bandwidth since the orthogonally polarized modes are degenerate. However, the double- and quadruple-ridged circular waveguides too have large bandwidth in applications where only symmetric discontinuities are present. It is found that the characteristic impedance of the quadruple-ridged circular waveguide decreases a little more rapidly with increased ridge penetration depth when compared to a double-ridged circular waveguide.

References

[1] R Behe and P. Brachat, "Compact duplexer-polarizer with semicircular waveguide," *IEEE Trans Antennas Propagat*, vol 39, pp. 1222–1224, Aug. 1991.

[2] D. A. Al-Mukhtar and J. E. Sitch, "Transmission-line matrix method with irregularly graded space," *IEE Proc*, vol 128, pt. H, no. 6, pp. 209–305, Dec. 1981.

[3] P. Daly, "Polar geometry waveguides by finite element methods," *IEEE Trans. Microwave Theory Tech.* vol. MTT-22, pp. 202–209, 1974.

[4] F. Canatan, "Cutoff wavenumbers of ridged circular waveguides via Ritz–Galerkin approach," *Electronic Lett.*, vol. 25, pp. 1036–1038, Aug. 89.

[5] B. M. Dillon and A. A. P Gibson, "Triple-ridged circular waveguides," *J. of Electromag. Waves Applicat.*, vol. 9, pp. 145–156, 1995.

[6] A. S. Omar, A. Jostingmeier, C. Rieckmann, and S. Lutgert, "Application of GSD technique to the analysis of slot-coupled waveguides," *IEEE Trans. Microwave Theory Tech.* vol. 42, pp. 2139–2148, Nov. 1994.

[7] M. H Chen, N. Tsandoulas, and F. G. Willwerth, "Modal characteristics of quadruple-ridged circular and square waveguides," *IIEEE Trans. Microwave Theory Tech* vol. MTT-22, pp. 801–804, Aug. 1974.

[8] W. Sun and C A Balanis, "Analysis and design of quadruple-ridged waveguides," *IEEE Trans. Microwave Theory Tech.* vol. 42, pp. 2201–2207, Dec. 1994.

[9] Y C. Shih, "The mode-matching method," in *Numerical Techniques for Microwave and Millimeter-wave Passive Structures*, T. Itoh, Ed New York: Wiley, 1989, pp. 592–621

[10] B. V. de la Filolie and R. Vahldieck, "Coaxial and circular waveguide bandpass filters using printed metal inserts," in *IEEE MTT-S Dig.*, 1992, pp. 905–908

[11] V. A. Labay and J. Bornemann, "Matrix singular value decomposition for pole free solutions of homogeneous matrix equations as applied to numerical modeling," *IEEE Microwave Guided Wave Lett.*, vol. 2, pp. 49–51, Feb. 1992.

[12] S. J. Skinner and G. L James, "Wide-band orthomode transducer," *IEEE Trans. Microwave Theory Tech.*, vol. 39, pp. 294–300, Feb. 1991.

[13] R. F. Harrington, *Time-Harmonic Electromagnetic Fields.* New York: McGraw-Hill, 1961.

[14] U. Balaji and R. Vahldieck, "Radial mode matching analysis of ridged circular waveguide," in *IEEE MTT-S Dig.*, May 1995, pp. 637–640.